

Article

Automatic High-Resolution Land Cover Production in Madagascar Using Sentinel-2 Time Series, Tile-Based Image Classification and Google Earth Engine

Meinan Zhang ¹, Huabing Huang ^{2,3} , Zhichao Li ¹, Kwame Oppong Hackman ^{4,5} ,
Chong Liu ^{2,3}, Roger Lala Andriamiarisoa ⁶, Tahiry Ny Aina Nomenjanahary Raherivelo ⁷,
Yanxia Li ⁸ and Peng Gong ^{1,*} 

¹ Ministry of Education Key Laboratory for Earth System Modeling, Department of Earth System, Science, Tsinghua University, Beijing 100084, China; zhangmn18@mails.tsinghua.edu.cn (M.Z.); lizc@igsnr.ac.cn (Z.L.)

² School of Geospatial Engineering and Science, Sun Yat-Sen University, Guangzhou 510275, China; huanghb@radi.ac.cn (H.H.); liuchong5@mail.sysu.edu.cn (C.L.)

³ Southern Marine Science and Engineering Guangdong Laboratory (Zhuhai), Zhuhai 519080, China

⁴ Data Management Department, WASCAL Competence Center, Ouagadougou 06 BP 9507, Burkina Faso; Hackman.k@wascal.org

⁵ Department of Environmental Management, University of Energy and Natural Resources, Sunyani BS-0061-2164, Ghana

⁶ Missouri Botanical Garden, Antananarivo 101, Madagascar; roger.andriamiarisoa@mobot.mg

⁷ Ministry of Environment and Sustainable Development, Antananarivo 101, Madagascar; trahevivo@bnc-redd.mg

⁸ International Bamboo and Rattan Organisation, Beijing 100102, China; yxli@inbar.int

* Correspondence: penggong@mail.tsinghua.edu.cn; Tel.: +86-010-62788023

Received: 11 October 2020; Accepted: 3 November 2020; Published: 8 November 2020



Abstract: Madagascar, one of Earth's biodiversity hotspots, is characterized by heterogeneous landscapes and huge land cover change. To date, fine, reliable and timely land cover information is scarce in Madagascar. However, mapping high-resolution land cover map in the tropics has been challenging due to limitations associated with heterogeneous landscapes, the volume of satellite data used, and the design of methodology. In this study, we proposed an automatic approach in which the tile-based model was used on each tile (defining an extent of $1^\circ \times 1^\circ$ as a tile) for mapping land cover in Madagascar. We combined spectral-temporal, textural and topographical features derived from all available Sentinel-2 observations (i.e., 11,083 images) on Google Earth Engine (GEE). We generated a 10-m land cover map for Madagascar, with an overall accuracy of 89.2% based on independent validation samples obtained from a field survey and visual interpretation of very high-resolution (0.5–5 m) images. Compared with the conventional approach (i.e., the overall model used in the entire study area), our method enables reduce the misclassifications between several land cover types, including impervious land, grassland and wetland. The proposed approach demonstrates a great potential for mapping land cover in other tropical or subtropical regions.

Keywords: land cover; tile-based model; big data; Sentinel-2; Google Earth Engine; Madagascar

1. Introduction

The characteristics of the earth's surface are determined by the dominant land cover categories such as impervious surface, vegetation, water, soil and permanent snow and glaciers [1]. Land cover maps provide fundamental information of the surface of the land. Accurate, timely land cover information is a

requisite for understanding how land cover changes affect biodiversity conservation [2–4], especially for tropical biodiversity hotspots [5]. It is also essential for other applications, for example, climate change studies [2,6] and environmental studies [7,8].

Madagascar, known as one of the Earth's biodiversity hotspots, is experiencing land cover change problems, leading to many environmental issues [9]. However, fine, reliable, and timely land cover maps with multiple land cover types for Madagascar are scarce. The available land cover maps for Madagascar have been undertaken over relatively regional areas such as a province [10] or focused on a single land cover class [11,12]. These products are not able to provide a detailed overview of the landscape on a national scale. Additionally, the other country-wide land cover products have several limitations, such as poor spatial consistency [13] and low spatial resolution [14], which is a disadvantage for the provision of reliable and finer land cover information of Madagascar. For example, the S2 prototype land cover 20-m map of Africa 2016 [15], which is a moderate-resolution map covering an entire continent for the year 2016, can be used for conservation of biodiversity, crop monitoring and climate modelling. However, this product has a low overall accuracy (OA) of 65% [14]. The low accuracy of the Madagascar-wide land cover map limits its use for various applications in the country. It is, therefore, essential to produce an improved and reliable country-wide land cover map of Madagascar using high-resolution satellite datasets.

Remote sensing has been widely recognized as the most economic and feasible approach to derive land cover information at large spatial scales [16–18]. Compared with Moderate Resolution Imaging Spectroradiometer (MODIS) and Landsat data with coarser spatial resolution, Sentinel-2 data are more suitable for fine scale classification of land cover types in the case of fragmented and small-patch land. Previous studies have shown that Sentinel-2 imagery has a strong ability to distinguish different land cover classes [19,20], and it outperforms other satellite imagery [21,22]. The classification results obtained using Sentinel-2 data with a spatial resolution of 10 m were able to capture the more detailed and fragmented land cover categories, especially for tropical regions. Tropical land cover classification based on remote sensing has been a challenging task. A major difficulty is the heterogeneous nature of land cover in tropical regions, especially for Madagascar due to its very rich, endemic and unique vegetation types [23]. Although the number of available methods for land cover mapping has been increasing, it is needed to be put into place to choose the appropriate classification method, especially for highly heterogeneous landscapes (e.g., Madagascar), which require further research efforts [24].

Since frequent cloud cover and inner errors of satellite sensors (e.g., the Scan Line Corrector failure of Landsat 7) have made earth observation data insufficient in tropical regions [25], in order to acquire and process a sufficient volume of satellite images, a cloud-based computational platform, such as Google Earth Engine (GEE), is needed [26]. GEE is a cloud-based geospatial analysis platform with the advantage of storage capacity and computing power, which allows users to easily access interactive remotely sensed images and algorithms [26]. A number of studies have shown good performance of GEE in mapping and monitoring different land cover types, such as forest [27], cropland [12], urban [28,29], wetland [30], and bamboo [31,32], from a local scale [33] to a global scale [34]. The huge data pool of GEE provides various satellite and long-term observations, which not only make it possible to use large amounts of remotely sensed data, but also to employ spectral–temporal information derived from the long-term time-series satellite data. Such spectral–temporal features are very beneficial for the discrimination of different land cover classes [35–37] because spatial variability and seasonal information (e.g., the phenological feature) can be captured with frequent and repeated observation over time. Although GEE has contributed to promoting the development of the forest measurement and monitoring program (e.g., reduced emissions from deforestation and forest degradation (REDD)), most researchers in Africa [38] and other developing countries do not realize its power in data accessibility and data-processing for large-scale land cover mapping, which is likely due to the lack of the applicable GEE-based land cover mapping frameworks for specific regions such as Madagascar. Therefore, more studies are needed to explore the applicability of the platform for Africa and to promote GEE utilization.

In this study, we used an automatic land cover mapping approach and designed the tile-based model to classify the corresponding region, which integrated high-resolution Sentinel-2 imagery in GEE to improve the 10-m resolution land cover mapping for the highly heterogeneous landscapes. We produced a 10-m land cover map of Madagascar for circa 2018. We then compared the performance of our proposed approach to that of the conventional method (i.e., one model is applied to the entire study area) using qualitative and quantitative approaches. We also explored the performance of employing big data in mapping highly heterogeneous areas. Finally, we estimated the performance of the finished land cover map by comparing it with the previous land cover maps of Madagascar.

2. Materials and Methods

A comprehensive overview of the methodology used for mapping heterogeneous landscape in Madagascar is shown in Figure 1. The sample collection, image preprocessing, feature selection, classification and post classification steps are presented in the following sub-sections.

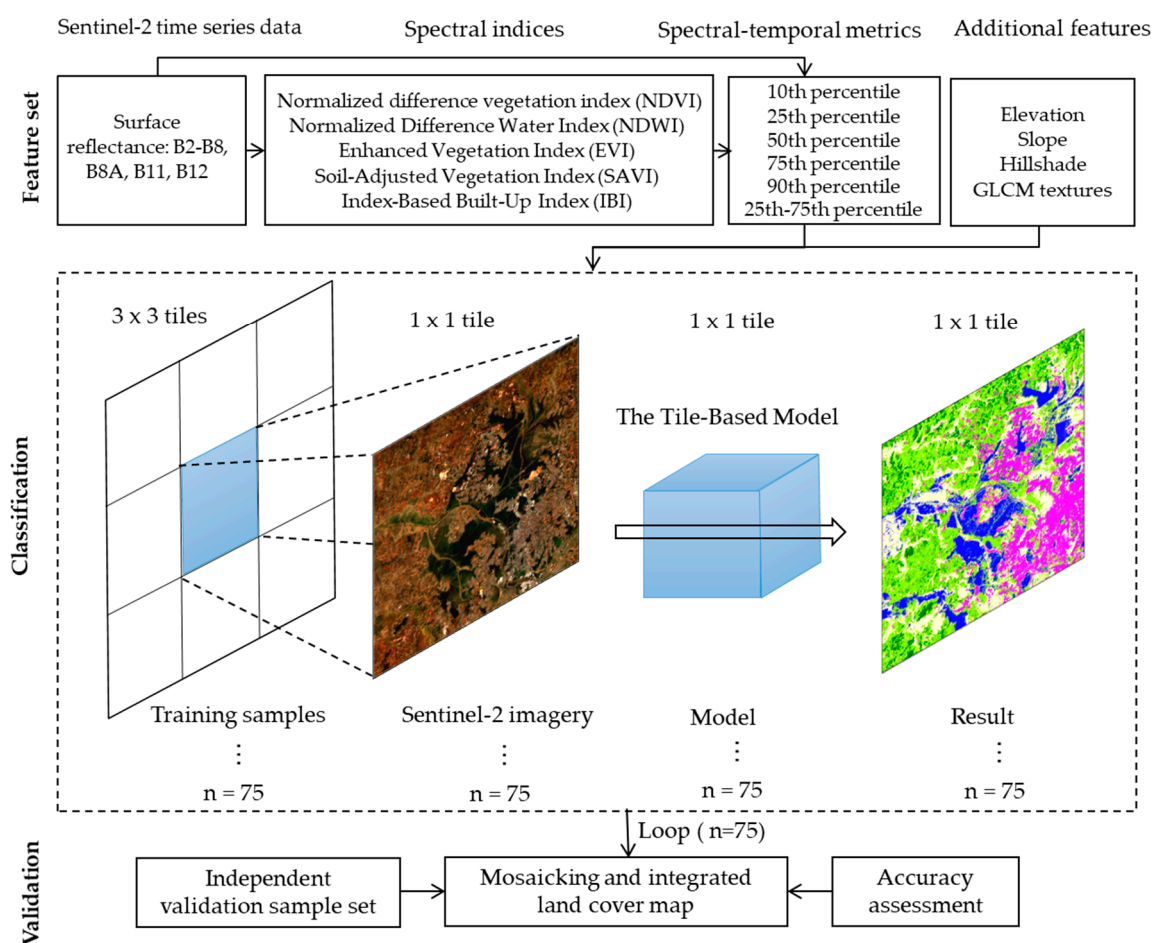


Figure 1. The workflow of the tile-based model used in this study for mapping highly heterogeneous land cover in Madagascar. One tile refers to an extent of $1^\circ \times 1^\circ$.

2.1. Sampling Strategy and Classification Scheme

Collecting accurate reference samples is a prerequisite to performing accurate land cover classification [39]. Insufficient and unrepresentative samples have been recognized as the main source of error in land cover classification [30]. In this study, the training and validation datasets were sampled independently using a hexagon random sampling strategy (see Figure 2) based on the prior knowledge provided by our extensive field campaigns and local experts. The hexagon-based equal-area random sampling scheme guaranteed the random and even distribution of different land

cover categories in Madagascar. We randomly selected ~10 points of the dominant land cover type within each hexagon cell as training samples, but in order to balance the proportion of land cover types with small areas such as impervious area, bare land, and wetland, several hexagons had unequal point numbers. All samples were selected uniformly across the entire island to avoid spatial correlation. For accuracy assessment, we selected random samples from sub-meter to 5-m very high-spatial resolution imagery (VHRI) as an independent validation set. Using geometry tools, samples were drawn in earth engine code editor through visual interpretation. Finally, the total numbers of training and validation samples were 9220 and 1278, respectively. The classification scheme included the following land cover classes: cropland, forest, grassland, shrubland, wetland, waterbody, impervious land and bare land, and their classification descriptions are presented in Table 1.

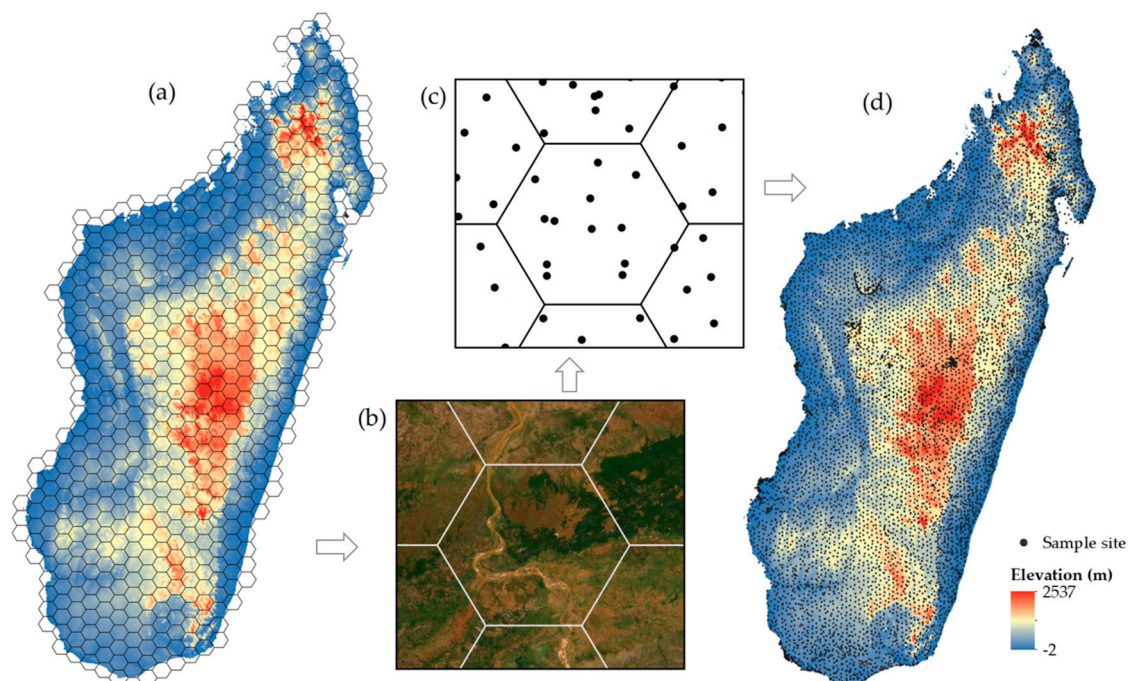


Figure 2. Schematic representation of the hexagon random sampling process in this study. Four steps: (a) generation of hexagons covering the whole study area; (b) visual interpretation of each hexagon overlaid on high-resolution Google Earth imagery; (c) selection of the location of land cover types; and (d) obtention of the sample set of the study area.

2.2. Image Processing and Feature Collection

The remotely sensed data are from the Sentinel 2 Surface Reflectance imagery archive available on GEE's data pool, with 10-m spatial resolution and 5-day temporal resolution. The GEE's cloud screening algorithm based on quality assessment bands (QA60) was applied in order to remove cloud and cloud shadow contaminated pixels for each of the Sentinel scenes covering Madagascar. All available images during the period of 2017–2019 (i.e., 11083 images in total) were used to generate the circa 2018 wall-to-wall cloud-free mosaics in order to reduce the influence of frequent cloud and less effective observation in Madagascar. JAXA's ALOS 30 m Digital Elevation Models (DEM) [40] are used to characterize the topographic characteristics of Madagascar.

We extracted the spectral-temporal features derived from the time series of Sentinel 2 observation and DEM data. Based on the surface reflectance bands, we calculated five spectral indices, including the Normalized Difference Vegetation Index (NDVI), the Enhanced Vegetation Index (EVI), the Normalized Difference Buildup Index (NDBI), the Normalized Difference Water Index (NDWI), and the Normalized Burn Ratio Index (NBRI). Moreover, we computed three terrain features (i.e., elevation, slope and hillshade) based on SRTM data. A multi-temporal data stack was generated for each of the ten

reflectance bands (i.e., B2-B8, B8A, B11, and B12), the four spectral indices using all available images, and the terrain features. Subsequently, for each pixel, the 10th, 25th, 50th, 75th, 90th and (25th–75th) percentiles were calculated. This approach of incorporating spectral-temporal metrics not only solves the problems of data gaps related to clouds, but also adds specific temporal information to the data, and can be helpful when identifying complex land cover classes such as cropland [35,37,41], especially for Madagascar.

Table 1. Descriptions of land cover classes included in this study.

Class	Description
Cropland	Areas characterized by clear traits of intensive human activity. This varies a lot from bare fields, seeding, and crop growing to harvesting. They can be easily identified if edges or textures are visible with sufficiently large land parcels. Fruit trees are classified as forests. Bare fields are classified as bare land. Pasture could be transitional from croplands to natural grasslands.
Forest	Areas where tree cover percentage classification to >15%; limits tree height classification to >3 m.
Grassland	Grassland for grazing and natural grassland are identifiable. Herbaceous cover percentage classification to >15%.
Shrubland	Areas characterized by a texture finer than tree canopies but coarser than grasslands, height between 5 and 0.3 m, and cover percentage classification to >15%.
Wetland	Areas dominated by natural and semi-natural aquatic or regularly flooded vegetation.
Waterbody	Areas dominated by natural waterbodies/artificial waterbodies.
Impervious	Areas dominated by artificial surfaces and associated area(s), primarily based on artificial cover such as asphalt, concrete, sand and stone, brick, glass, and other cover materials.
Bare land	Areas where vegetation is hardly observable but dominated by exposed soil, sand, gravel, and rock backgrounds.

We also computed five textural features of NDVI based on gray-level co-occurrence matrix (GLCM) to enlarge the discrepancy of different land cover categories, including contrast, which measures the local contrast of an image; correlation, measuring the correlation between pairs of pixels; inverse difference moment, measuring the homogeneity; entropy, measuring the randomness of a gray-level distribution; and angular second moment, which measures the number of repeated pairs. In addition, three terrain factors—elevation, hillshade and slope, were included into the feature set.

2.3. Classification and Accuracy Assessment

Due to the enormous size of the 10-m Sentinel-2 time series data over the entire area of Madagascar, it is essential to use a powerful calculation tool, the GEE cloud platform, for image processing, feature collection, and classification. With regard to the highly heterogeneous land cover in Madagascar, we designed the tile-based classification model to carry out the classification task of corresponding tiles (defining an extent of $1^\circ \times 1^\circ$ as a tile) to solve the difficulty in mapping tropically heterogeneous landscapes over the large spatial scale. Specifically, we first generated the $1^\circ \times 1^\circ$ tiles over the whole island, resulting in 75 tiles. Each tile-based model was trained using the training samples within this tile and its neighboring 8 tiles (i.e., $3^\circ \times 3^\circ$, see Figure 1), which allowed each tile-based model to have enough samples to be calibrated, subsequently ensuring its predictive ability. Then, we carried out the classification procedure of the corresponding tile. The procedure was repeated for each tile in the study area, which made the classification model more specific to the corresponding areas with larger differences of land cover types. The random forest (RF) classifier was chosen to implement the classification task in this study, with a tree number of 200, as the RF algorithm is able to process massive high-dimensional data while maintaining high accuracy [42,43], and it is also resistant to noise and overfitting issues [44]. The parameters of RF have little influence on classification accuracy [45], and the number of trees was thus adjusted in this study.

For evaluating the predictive accuracy across the classes as well as the overall accuracy, a confusion matrix was produced using the independent validation data, which enable the provision of a cross-tabulation of the validation samples against the corresponding mapped pixel classes. This allowed for an assessment of the producer accuracy (the number of correctly classified pixels divided by the total number of true pixels in a given class) and the user accuracy (the number of correctly classified pixels divided by the total predicted pixels within that class), which were calculated to assess the accuracy of the final land cover map.

2.4. Comparison Analysis among Products and Methods

We compared our produced land cover map for Madagascar (namely the MDG LC-10 map) with two existing high-resolution land cover products of Madagascar for evaluating the proposed approach in this study, including the S2 prototype land cover 20-m map of Africa 2016 (namely the Climate Change Initiative (CCI) Africa LC-20 map) and the first 10-m resolution global land cover map (namely the FROM-GLC10) produced by the Tsinghua University (Gong et al., 2019). The CCI Africa LC-20 map was produced by the European Space Agency (ESA) Climate Change Initiative (CCI) at 20 m over Africa based on one year of Sentinel-2A observations from December 2015 to December 2016. This product has a legend of eleven types and accuracy varied from 44% (for South Africa) to 91% (for Gabon) [15]. The FROM-GLC10 dataset was produced by the Tsinghua University using Sentinel-2 images to generate a 10-m resolution global land cover map [34]. The classification system of FROM-GLC10 includes ten land cover classes that are described in Gong, et al. [46], and its overall accuracy is 72.76%. Furthermore, we compared our MDG LC-10 map with the sub-meter to 5-m very high spatial resolution imagery from Google Earth, representing the real land cover surface.

In addition, we also used qualitative and quantitative approaches to evaluate the performance of the proposed method in this study. In general, a classification model is used to classify land cover types of the whole study area (namely “the overall model”). We compared our proposed method (i.e., the one tile-based model is applied to one tile) with the method used by the overall model (i.e., one model is applied to the entire study area).

3. Results and Discussion

3.1. Ten-Meter Circa 2018 LC Map of Madagascar

We produced a contemporary land cover map of Madagascar at 10-m spatial resolution for circa 2018 using Sentinel-2 big data and tile-based random forest classification implemented in the GEE platform (Figure 1), and zoomed in on major locations in Madagascar to illustrate the mapping performance (Figure 3b–d). This land cover map was produced over eight dominant classes, with a good performance in terms of spatial consistency on a national scale. An accuracy assessment was implemented using the independent validation dataset. Based on the confusion matrix shown in Table 2, the overall accuracy and Kappa of the resultant map were 89.2% and 0.87, respectively, demonstrating good potential of the proposed approach for automatic land cover mapping for highly heterogeneous landscapes. As shown in Figure 3a, the proportions of eight land cover classes over the whole island were as follows: cropland, 7.2%; forest, 21.7%; grassland, 52.3%; shrubland, 17.2%; wetland, 0.3%; waterbody, 0.7%; impervious land, 0.2%; and bare land, 0.5%. Due to large heterogeneity of tropical vegetation, it is difficult to map the fine and detailed land cover in Madagascar using coarser spatial resolution satellite data (e.g., Landsat and MODIS images). Previous studies have proved that the Sentinel-2 derived land cover classifications have an advantage in mapping extensive and smaller-sized cover types [34,47,48], especially for tropical regions. Our results also provided evidence that Sentinel-2 imagery can be applied to accurately delineate the complex and heterogeneous land cover types in Madagascar. Although Sentinel-2 satellite imagery is good for monitoring land surface at a higher spatial resolution, the accuracy assessment indicated that croplands are easily confused with grassland, and grassland is more likely to be misclassified as bare land (Table 2).

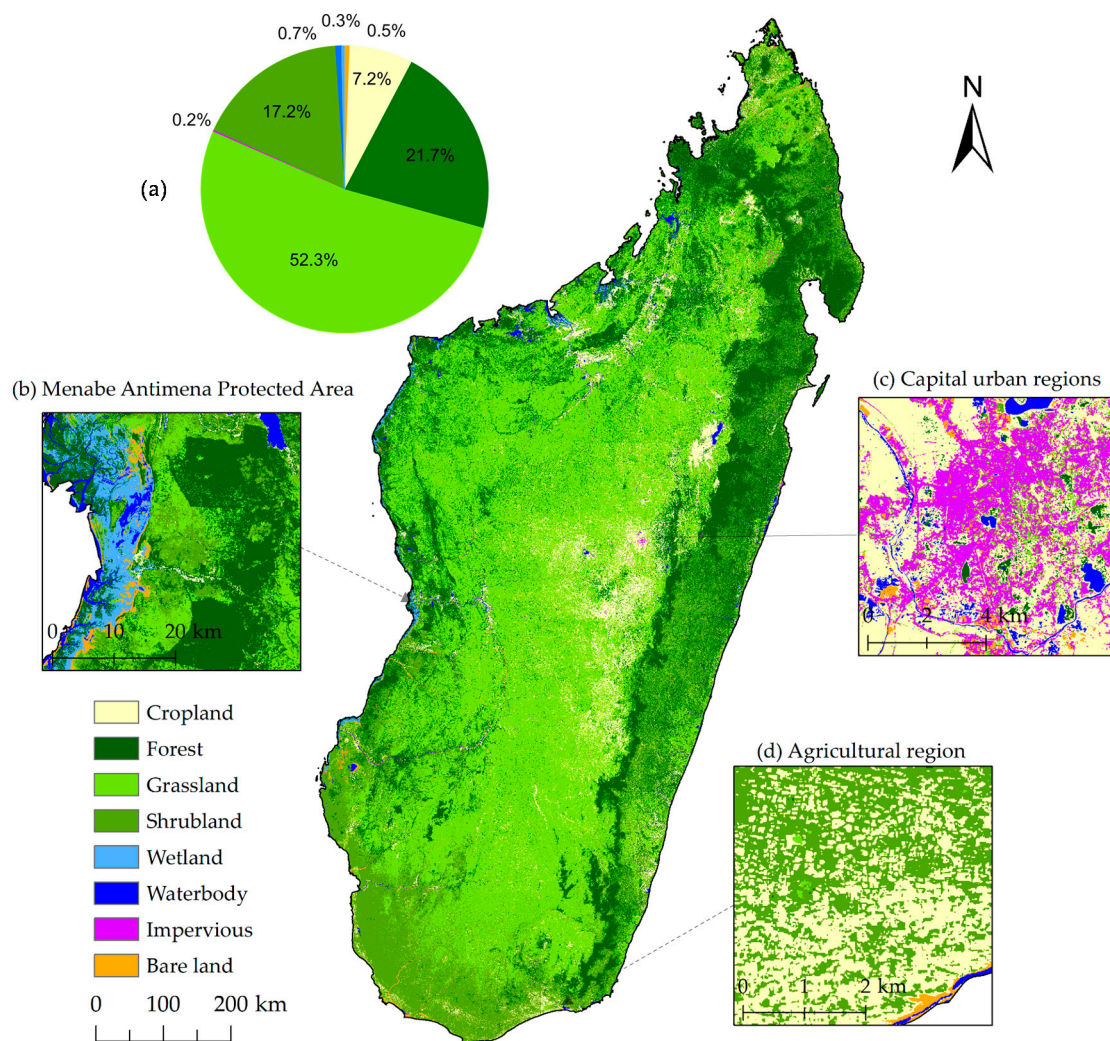


Figure 3. Overview of the 10-m circa 2018 land cover map of Madagascar (i.e., the MDG LC-10 map) derived from the Sentinel-2 dataset. (a) The proportions of the eight major land cover classes over the entire island. The zoomed in windows show the details ranging from the landscape view (b), the urban structure (c), and the fine grain land cover patterns (d).

3.2. Comparisons among Google Earth Images, Two Available High-Resolution Land Cover Maps of Madagascar and the MDG LC-10 Land Cover Map

It was observed that there was a significant improvement in the MDG LC-10 map produced in this study when compared with two available high-resolution land cover maps (i.e., the CCI Africa LC-20 map and the FROM-GLC10 map) and very high spatial resolution imageries from Google Earth. For instance, plenty of misclassified croplands occurred in forest-dominant areas in the CCI Africa LC-20 map (Figure 4a), which were improved in the FROM-GLC10 map but not completely solved. However, this phenomenon was well avoided in the MDG LC-10 map. This can be explained by the use of the tile-based model, which effectively prevented the occurrence of some specific land cover types such as cropland and impervious areas that are not originally available in one tile (i.e., an extent of $1^\circ \times 1^\circ$). The strength of our method is also reflected in the way it addresses the misclassified impervious type in the other land cover maps. As an example, in Figure 4b, the FROM-GLC10 map wrongly classified lots of grassland areas as impervious surface. Furthermore, it is evident in Figure 3b that the wetland class was well identified in the MDG LC-10 map, while the CCI Africa LC-20 map and the FROM-GLC10 map failed. Moreover, Figure 4c demonstrates that the MDG LC-10 map provided more detailed and accurate extents of impervious areas than the other land cover maps. This is likely the result

of introducing the texture features in our approach. Moreover, we also quantified the performances between our map and other maps using the independent validation samples, and then compared their producer accuracies. Figure 5 indicates that the producer accuracies of the eight land cover classes of the MDG LC-10 map (average PA = 88.2%) outperformed those of the CCI Africa LC-20 map (average producer accuracy (PA) = 60.8%) and the FROM-GLC10 map (average PA = 65.9%). Based on these comparisons, we demonstrate that the 10-m resolution land cover map generated in this study (i.e., the MDG LC-10 map) is able to provide a more reliable land cover information than the FROM-GLC10 map and more detailed land cover information than the CCI Africa LC-20 map.

Table 2. Accuracy assessment of the MDG LC-10 map’s confusion matrix based on the independent validation samples.

Reference Class	Mapped Class								Total	PA(%)
	Cropland	Forest	Grassland	Shrubland	Wetland	Waterbody	Impervious	Bare Land		
Cropland	183	1	20	14	1	0	1	0	220	83.2
Forest	0	206	6	11	0	0	0	0	223	92.4
Grassland	4	3	235	1	1	0	0	0	244	96.3
Shrubland	2	15	12	114	0	0	0	0	143	79.7
Wetland	5	0	2	0	38	2	0	0	47	80.9
Waterbody	3	0	0	0	0	89	0	3	95	93.7
Impervious	0	0	12	2	0	0	158	2	174	90.8
Bare land	3	0	6	1	0	4	1	117	132	88.6
Total	200	225	293	143	40	95	160	122	1278	
UA(%)	91.5	91.6	80.2	79.7	95.0	93.7	98.8	95.9		
OA(%) : 89.2;							Kappa : 0.87.			

Note: PA = producer accuracy; UA = user accuracy; OA = overall accuracy.

3.3. Comparisons of the Overall Model vs. the Tile-Based Model

The advantages of the proposed method in this study are mainly highlighted in two aspects: (1) the use of tile-based model makes the classification more specific to those regions with greater heterogeneity; (2) the employment of big data from GEE provides more observation information, which is used for delineating more detailed characteristics between different land cover classes.

In large-scale land cover mapping, the misclassification of land cover types with similar spectra (e.g., cropland and grassland) is common, and is more severe when classifying areas with high spatial heterogeneity and fragmented landscapes such as Madagascar. The proposed approach in this study demonstrated great potential in addressing this problem. This is because the tile-based model employed in this study made the classification more specific and targeted different heterogeneous landscapes. However, the conventional approach, which adopts a overall classification model, does not possess this advantage. It is evident from Figure 6 that, when the conventional method is used, incorrectly identified cropland (Figure 6b) and impervious land (Figure 6e) classes occur in the results, while the proposed methodology correctly identifies these classes (Figure 6c,f). This shows that the proposed method has great potential to improve the phenomenon of misclassification in the two land cover types—cropland and impervious area.

In addition to the visual comparison, a statistical comparison was made between the land cover maps produced using our proposed method and the conventional method. In this regard, the maps were evaluated based on the independent validation samples described in Section 2.1. Figure 7 represents the producer accuracies (PAs) of the eight different land cover classes identified in the classification results of our proposed method (i.e., the one tile-based model is applied to one tile) and the method based on a overall model (i.e., one model is applied to the entire study area). We found

that the PAs of all land cover classes from our proposed method, except for forest, were higher than that for the conventional method. The average PA for our proposed method was 88.2%, while the traditional method had a lower average accuracy of 84.8%. The highest difference in PA was observed for waterbody, followed by wetland and bare land, indicating the advantage of employing a tile-based model for accurately mapping the frequently changing land cover types. For the other classes, the differences in PA varied between 1% and 6%, demonstrating the efficiency of applying the tile-based model for the Madagascar-wide land cover mapping.

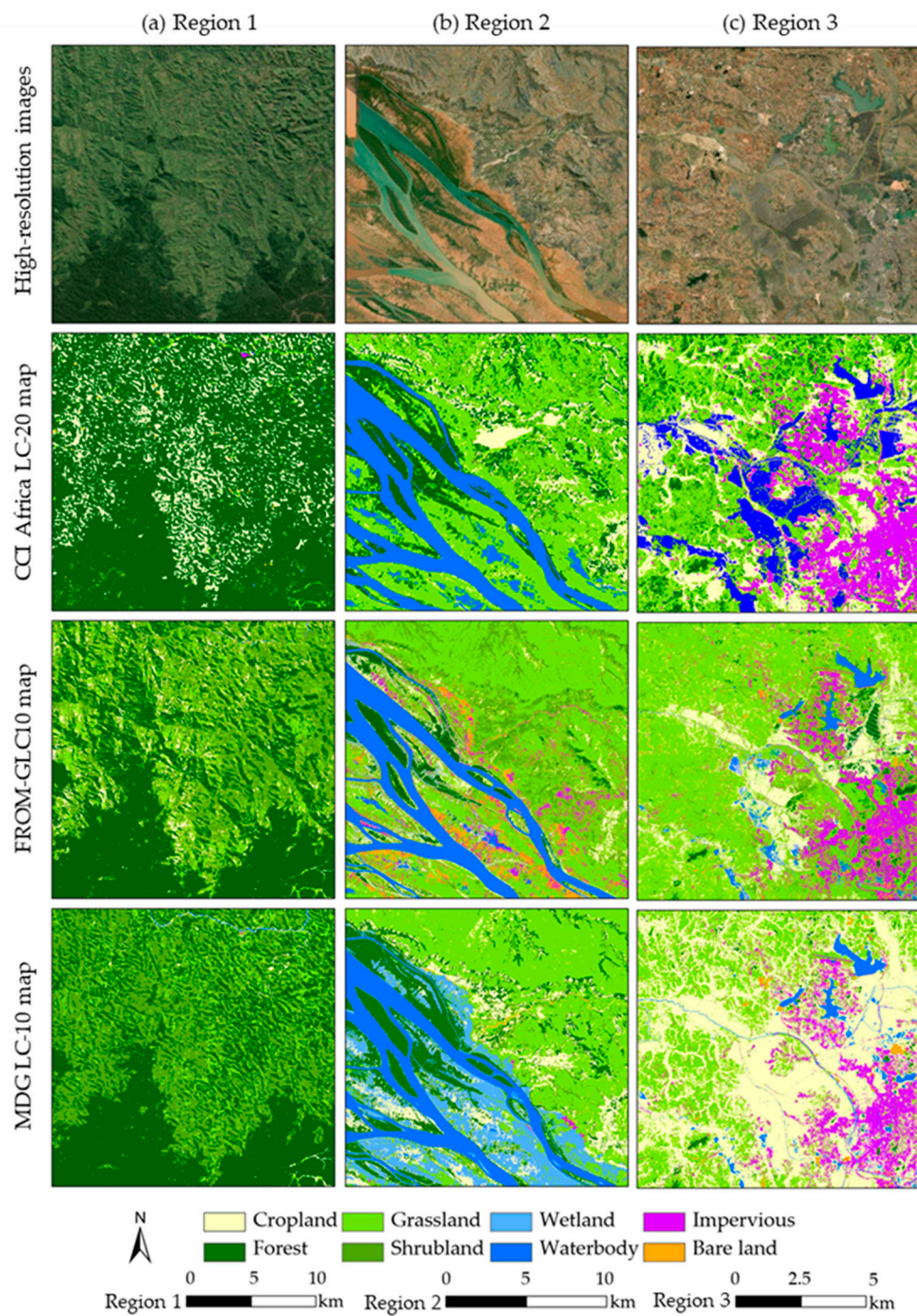


Figure 4. Visual comparison of three zoomed areas (a–c) among the MDG LC-10 map, two high resolution land cover maps (i.e., the CCI Africa LC-20 map and the FROM-GLC10 map) and very high resolution imagery from Google Earth.

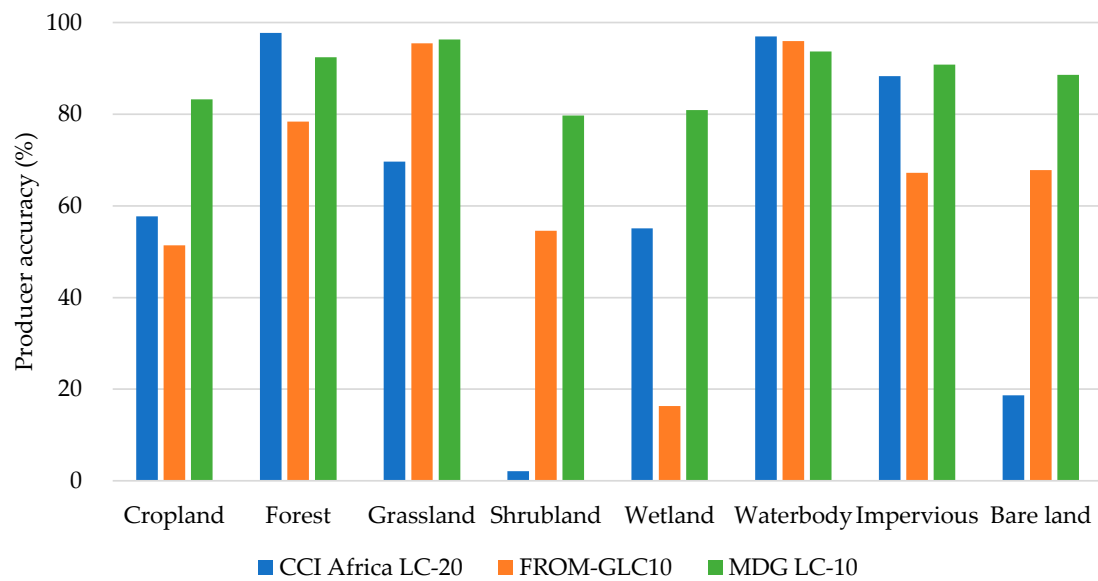


Figure 5. Statistical comparison of producer accuracies (PAs) of the available high-resolution land cover maps for Madagascar and the map produced in this study.

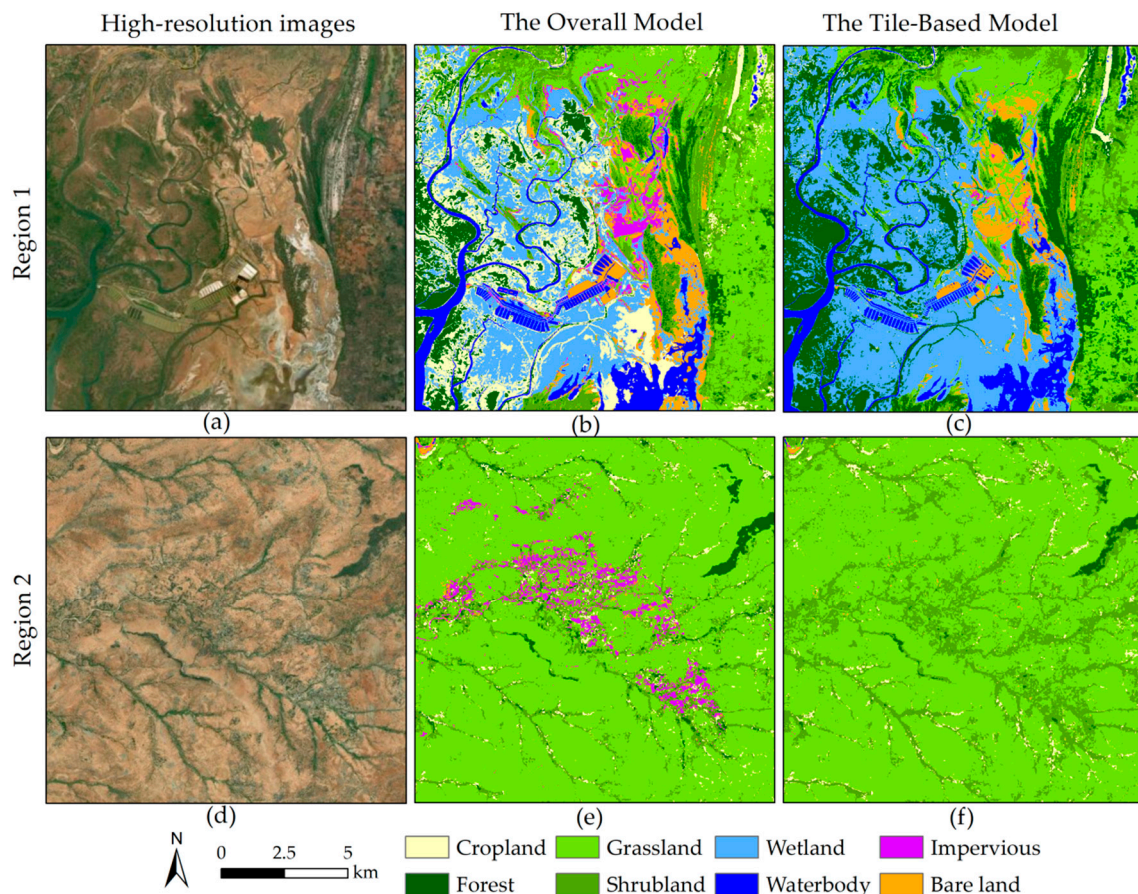


Figure 6. Examples of comparison of the classification performance using our proposed method (i.e., the tile-based model) (c,f) in this study and the conventional method (i.e., the overall model) (b,e). (a,d) are zoomed high-resolution images from Google Earth. Region 1 exhibits an improvement in the misclassification between cropland and wetland. Region 2 shows that the issue of impervious areas misclassification is improved.

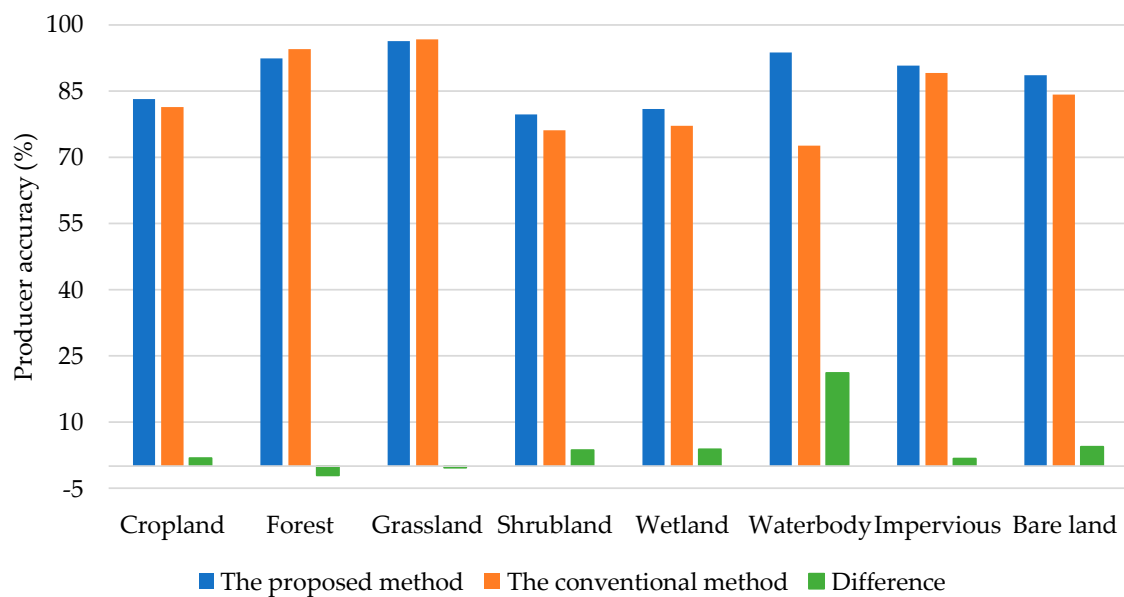


Figure 7. Statistical comparison of producer accuracies (PAs) for the proposed method (i.e., the one tile-based model is applied to one tile) and the conventional method (i.e., one model is applied to the entire study area). The blue and orange bars represent the PAs of eight land cover classes, and the green bars indicate that the differences in PAs.

The use of big data from GEE also exhibited an advantage in mapping land cover in Madagascar. Based on a visual interpretation and comparison with high-resolution satellite images, it was observed that the proposed big data processing method in this study provided a visually satisfactory depiction of nearly all classes (Figure 8). The results showed that there were lots of misclassified impervious area in the classification results using the Sentinel-2 images with cloud cover below 10% (i.e., 4900 images) as input, while a large improvement was observed when all available Sentinel-2 images covering Madagascar (i.e., 11,083 images) were used as input (Figure 8a–c). Moreover, we also found that the usage of big data enhanced the ability to differentiate bare land and shrubland as well as grassland, compared with the fewer Sentinel-2 images used in the classification (Figure 8d,e). This main reason for this observation is that long-term and dense observations are able to provide seasonal phenological information. Our results demonstrate that the use of big data for land cover mapping makes the classification results finer and more accurate, which highlights the advantages of GEE in providing a large volume satellite imagery pool and data processing ability for mapping tropically heterogeneous land cover. The usage and processing of large amounts of satellite-based data is becoming more difficult as the spatial resolution of images from new sensors increases [26,49,50]. Furthermore, for tropical regions, the usable and efficient observations are fewer than other regions of the world mainly due to frequent cloud cover. GEE applied here overcame the computational challenge of handling large earth observation data, which is favorable for tropical land cover mapping due to its fewer surface observations.

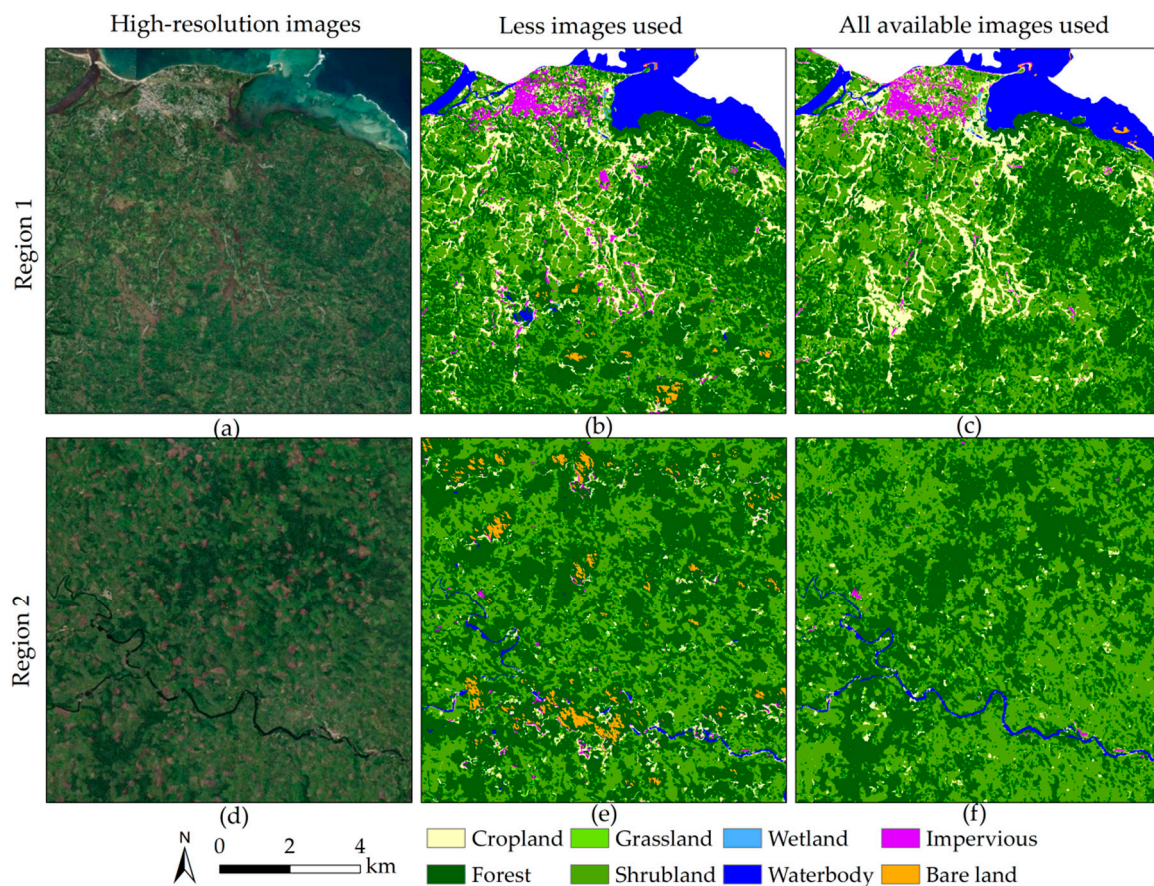


Figure 8. Examples of comparisons of the classification performances using Sentinel-2 images with cloud cover below 10% (i.e., $n = 4900$ images, **b,e**) and using all available Sentinel-2 images (i.e., $n = 11,083$ images, **c,f**) over the entire island. (**a,d**) were derived from high-resolution Google earth imagery.

4. Conclusions

In this study, we developed a novel classification framework for highly heterogeneous landscape, in which the tile-based model was used to classify the complex land cover types of Madagascar. Using a combination of field survey and satellite observation data, we produced the first Madagascar land cover map with a 10-m spatial resolution. The GEE platform provided the tools to handle high computation requirements and to extract spectral-temporal features from the large time-series images across the spatial extent of the country. The overall accuracy of 89.2% obtained for the map demonstrates the high potential of the proposed method for producing land cover maps in tropical regions. Moreover, by comparing the land cover map produced in this study with those previously generated by CCI and Tsinghua University, the proposed method clearly presents a significantly improved land cover map (i.e., MDG LC-10) of Madagascar. This map will greatly contribute to many fields and, thus, can be incorporated into various applications, such as the inventory of land use status and biodiversity conservation. Additionally, the methodology presented in this study offers an efficient approach for producing Madagascar-wide land cover maps and also makes it possible to automatically produce annual up-to-date country-wide land cover maps, enabling users (e.g., land managers and policy makers) to investigate the dynamic of land cover over longer time periods. We recommend this approach especially for regions dominated by heterogeneous land cover classes and frequent cloud cover.

Author Contributions: Conceptualization, M.Z. and P.G.; methodology, M.Z.; software, M.Z.; validation, M.Z.; formal analysis, M.Z., H.H., Z.L. and P.G.; data curation, M.Z., Z.L., R.L.A., T.N.A.N.R., and Y.L.; writing—original draft preparation, M.Z.; writing—review and editing, M.Z., Z.L., K.O.H., H.H., C.L. and P.G.; visualization, M.Z.; supervision, P.G.; funding acquisition, P.G. All authors have read and agreed to the published version of the manuscript.

Funding: This research was funded by the Ministry of Science and Technology of the People’s Republic of China, grant number 2016YFA0600104.

Acknowledgments: We thank the International Bamboo and Rattan Organisation, the Ministry of Environment and Sustainable Development, Madagascar and the Missouri Botanical Garden, Madagascar for facilitating our filed work in Madagascar.

Conflicts of Interest: The authors declare no conflict of interest.

References

- Gómez, C.; White, J.C.; Wulder, M.A. Optical remotely sensed time series data for land cover classification: A review. *ISPRS J. Photogramm. Remote Sens.* **2016**, *116*, 55–72. [[CrossRef](#)]
- Hanna, D.E.; Raudsepp-Hearne, C.; Bennett, E.M. Effects of land use, cover, and protection on stream and riparian ecosystem services and biodiversity. *Conserv. Biol.* **2020**, *34*, 244–255. [[CrossRef](#)]
- Shumba, T.; De Vos, A.; Biggs, R.; Esler, K.J.; Ament, J.M.; Clements, H.S. Effectiveness of private land conservation areas in maintaining natural land cover and biodiversity intactness. *Glob. Ecol. Conserv.* **2020**, *22*, e00935. [[CrossRef](#)]
- Condro, A.A.; Prasetyo, L.B.; Rushayati, S.B. Short-term projection of Bornean orangutan spatial distribution based on climate and land cover change scenario. In Proceedings of the Sixth International Symposium on LAPAN-IPB Satellite, Bogor, Indonesia, 24 December 2019; p. 113721B.
- Heilmayr, R.; Echeverria, C.; Lambin, E.F. Impacts of Chilean forest subsidies on forest cover, carbon and biodiversity. *Nat. Sustain.* **2020**, 1–9. [[CrossRef](#)]
- Niu, X.; Tang, J.; Wang, S.; Fu, C. Impact of future land use and land cover change on temperature projections over East Asia. *Clim. Dyn.* **2019**, *52*, 6475–6490. [[CrossRef](#)]
- Birhanu, A.; Masih, I.; van der Zaag, P.; Nyssen, J.; Cai, X. Impacts of land use and land cover changes on hydrology of the Gumara catchment, Ethiopia. *Phys. Chem. Earth Parts A/B/C* **2019**, *112*, 165–174. [[CrossRef](#)]
- Yu, Z.; Lu, C.; Tian, H.; Canadell, J.G. Largely underestimated carbon emission from land use and land cover change in the conterminous United States. *Glob. Chang. Biol.* **2019**, *25*, 3741–3752. [[CrossRef](#)]
- Jones, J.P.; Ratsimbazafy, J.; Ratsifandrihamanana, A.N.; Watson, J.E.; Andrianandrasana, H.T.; Cabeza, M.; Cinner, J.E.; Goodman, S.M.; Hawkins, F.; Mittermeier, R.A. Last chance for Madagascar’s biodiversity. *Nat. Sustain.* **2019**, *2*, 350. [[CrossRef](#)]
- Dupuy, S.; Defrise, L.; Lebourgeois, V.; Gaetano, R.; Burnod, P.; Tonneau, J.-P. Analyzing Urban Agriculture’s Contribution to a Southern City’s Resilience through Land Cover Mapping: The Case of Antananarivo, Capital of Madagascar. *Remote Sens.* **2020**, *12*, 1962. [[CrossRef](#)]
- Harper, G.J.; Steininger, M.K.; Tucker, C.J.; Juhn, D.; Hawkins, F. Fifty years of deforestation and forest fragmentation in Madagascar. *Environ. Conserv.* **2007**, 325–333. [[CrossRef](#)]
- Xiong, J.; Thenkabail, P.S.; Gumma, M.K.; Teluguntla, P.; Poehnel, J.; Congalton, R.G.; Yadav, K.; Thau, D. Automated cropland mapping of continental Africa using Google Earth Engine cloud computing. *ISPRS J. Photogramm. Remote Sens.* **2017**, *126*, 225–244. [[CrossRef](#)]
- Li, Q.; Qiu, C.; Ma, L.; Schmitt, M. Mapping the Land Cover of Africa at 10 m Resolution from Multi-Source Remote Sensing Data with Google Earth Engine. *Remote Sens.* **2020**, *12*, 602. [[CrossRef](#)]
- Lesiv, M.; Fritz, S.; McCallum, I.; Tsendbazar, N.; Herold, M.; Pekel, J.-F.; Buchhorn, M.; Smets, B.; Van De Kerchove, R. *Evaluation of ESA CCI Prototype Land Cover Map at 20*; International Institute for Applied Systems Analysis: Laxenburg, Austria, 2017.
- Ramoino, F.; Pera, F.; Arino, O. *The S2 Prototype LC Map at 20 m of Africa 2016*; European Space Agency: Paris, France, 2016.
- Beamish, A.; Reynolds, M.K.; Epstein, H.; Frost, G.V.; Macander, M.J.; Bergstedt, H.; Bartsch, A.; Kruse, S.; Miles, V.; Tanis, C.M. Recent trends and remaining challenges for optical remote sensing of Arctic tundra vegetation: A review and outlook. *Remote Sens. Environ.* **2020**, *246*, 111872. [[CrossRef](#)]

17. Gong, P. Remote sensing of environmental change over China: A review. *Chin. Sci. Bull.* **2012**, *57*, 2793–2801. [[CrossRef](#)]
18. Weiss, M.; Jacob, F.; Duveiller, G. Remote sensing for agricultural applications: A meta-review. *Remote Sens. Environ.* **2020**, *236*, 111402. [[CrossRef](#)]
19. Rapinel, S.; Mony, C.; Lecoq, L.; Clement, B.; Thomas, A.; Hubert-Moy, L. Evaluation of Sentinel-2 time-series for mapping floodplain grassland plant communities. *Remote Sens. Environ.* **2019**, *223*, 115–129. [[CrossRef](#)]
20. Vaudour, E.; Gomez, C.; Fouad, Y.; Lagacherie, P. Sentinel-2 image capacities to predict common topsoil properties of temperate and Mediterranean agroecosystems. *Remote Sens. Environ.* **2019**, *223*, 21–33. [[CrossRef](#)]
21. Korhonen, L.; Packalen, P.; Rautiainen, M. Comparison of Sentinel-2 and Landsat 8 in the estimation of boreal forest canopy cover and leaf area index. *Remote Sens. Environ.* **2017**, *195*, 259–274. [[CrossRef](#)]
22. Astola, H.; Häme, T.; Sirro, L.; Molinier, M.; Kilpi, J. Comparison of Sentinel-2 and Landsat 8 imagery for forest variable prediction in boreal region. *Remote Sens. Environ.* **2019**, *223*, 257–273. [[CrossRef](#)]
23. Koechlin, J. Flora and vegetation of Madagascar. In *Biogeography and Ecology in Madagascar*; Springer: Dordrecht, The Netherlands, 1972; pp. 145–190.
24. Phiri, D.; Simwanda, M.; Salekin, S.; Nyirenda, V.R.; Murayama, Y.; Ranagalage, M. Sentinel-2 Data for Land Cover/Use Mapping: A Review. *Remote Sens.* **2020**, *12*, 2291. [[CrossRef](#)]
25. Saah, D.; Tenneson, K.; Matin, M.; Uddin, K.; Cutter, P.; Poortinga, A.; Ngyuen, Q.H.; Patterson, M.; Johnson, G.; Markert, K. Land cover mapping in data scarce environments: Challenges and opportunities. *Front. Environ. Sci.* **2019**, *7*, 150. [[CrossRef](#)]
26. Gorelick, N.; Hancher, M.; Dixon, M.; Ilyushchenko, S.; Thau, D.; Moore, R. Google Earth Engine: Planetary-scale geospatial analysis for everyone. *Remote Sens. Environ.* **2017**, *202*, 18–27. [[CrossRef](#)]
27. Chen, B.; Xiao, X.; Li, X.; Pan, L.; Doughty, R.; Ma, J.; Dong, J.; Qin, Y.; Zhao, B.; Wu, Z. A mangrove forest map of China in 2015: Analysis of time series Landsat 7/8 and Sentinel-1A imagery in Google Earth Engine cloud computing platform. *ISPRS J. Photogramm. Remote Sens.* **2017**, *131*, 104–120. [[CrossRef](#)]
28. Li, X.; Gong, P.; Zhou, Y.; Wang, J.; Bai, Y.; Chen, B.; Hu, T.; Xiao, Y.; Xu, B.; Yang, J. Mapping global urban boundaries from the global artificial impervious area (GAIA) data. *Environ. Res. Lett.* **2020**, *15*, 094044. [[CrossRef](#)]
29. Hackman, K.O.; Li, X.; Asenso-Gyambibi, D.; Asamoah, E.A.; Nelson, I.D. Analysis of geo-spatiotemporal data using machine learning algorithms and reliability enhancement for urbanization decision support. *Int. J. Digit. Earth* **2020**, 1–16. [[CrossRef](#)]
30. Amani, M.; Mahdavi, S.; Afshar, M.; Brisco, B.; Huang, W.; Mohammad Javad Mirzadeh, S.; White, L.; Banks, S.; Montgomery, J.; Hopkinson, C. Canadian wetland inventory using Google Earth engine: The first map and preliminary results. *Remote Sens.* **2019**, *11*, 842. [[CrossRef](#)]
31. Liu, C.; Xiong, T.; Gong, P.; Qi, S. Improving large-scale moso bamboo mapping based on dense Landsat time series and auxiliary data: A case study in Fujian Province, China. *Remote Sens. Lett.* **2018**, *9*, 1–10. [[CrossRef](#)]
32. Zhang, M.; Gong, P.; Qi, S.; Liu, C.; Xiong, T. Mapping bamboo with regional phenological characteristics derived from dense Landsat time series using Google Earth Engine. *Int. J. Remote Sens.* **2019**, *40*, 9541–9555. [[CrossRef](#)]
33. Huang, H.; Chen, Y.; Clinton, N.; Wang, J.; Wang, X.; Liu, C.; Gong, P.; Yang, J.; Bai, Y.; Zheng, Y. Mapping major land cover dynamics in Beijing using all Landsat images in Google Earth Engine. *Remote Sens. Environ.* **2017**, *202*, 166–176. [[CrossRef](#)]
34. Gong, P.; Liu, H.; Zhang, M.; Li, C.; Wang, J.; Huang, H.; Clinton, N.; Ji, L.; Li, W.; Bai, Y.; et al. Stable classification with limited sample: Transferring a 30-m resolution sample set collected in 2015 to mapping 10-m resolution global land cover in 2017. *Sci. Bull.* **2019**, *64*, 370–373. [[CrossRef](#)]
35. Pasquarella, V.J.; Holden, C.E.; Woodcock, C.E. Improved mapping of forest type using spectral-temporal Landsat features. *Remote Sens. Environ.* **2018**, *210*, 193–207. [[CrossRef](#)]
36. Pflugmacher, D.; Rabe, A.; Peters, M.; Hostert, P. Mapping pan-European land cover using Landsat spectral-temporal metrics and the European LUCAS survey. *Remote Sens. Environ.* **2019**, *221*, 583–595. [[CrossRef](#)]
37. Schug, F.; Frantz, D.; Okujeni, A.; van der Linden, S.; Hostert, P. Mapping urban-rural gradients of settlements and vegetation at national scale using Sentinel-2 spectral-temporal metrics and regression-based unmixing with synthetic training data. *Remote Sens. Environ.* **2020**, *246*, 111810. [[CrossRef](#)] [[PubMed](#)]
38. Tamiminia, H.; Salehi, B.; Mahdianpari, M.; Quackenbush, L.; Adeli, S.; Brisco, B. Google Earth Engine for geo-big data applications: A meta-analysis and systematic review. *ISPRS J. Photogramm. Remote Sens.* **2020**, *164*, 152–170. [[CrossRef](#)]

39. Li, C.; Wang, J.; Wang, L.; Hu, L.; Gong, P. Comparison of classification algorithms and training sample sizes in urban land classification with Landsat thematic mapper imagery. *Remote Sens.* **2014**, *6*, 964–983. [[CrossRef](#)]
40. Tadono, T.; Nagai, H.; Ishida, H.; Oda, F.; Naito, S.; Minakawa, K.; Iwamoto, H. Generation of the 30 M-mesh global digital surface model by ALOS PRISM. *Int. Arch. Photogramm. Remote Sens. Spat. Inf. Sci.* **2016**, *41*. [[CrossRef](#)]
41. Leinenkugel, P.; Deck, R.; Huth, J.; Ottinger, M.; Mack, B. The potential of open geodata for automated large-scale land use and land cover classification. *Remote Sens.* **2019**, *11*, 2249. [[CrossRef](#)]
42. Belgiu, M.; Drăguț, L. Random forest in remote sensing: A review of applications and future directions. *ISPRS J. Photogramm. Remote Sens.* **2016**, *114*, 24–31. [[CrossRef](#)]
43. Rodriguez-Galiano, V.F.; Ghimire, B.; Rogan, J.; Chica-Olmo, M.; Rigol-Sanchez, J.P. An assessment of the effectiveness of a random forest classifier for land-cover classification. *ISPRS J. Photogramm. Remote Sens.* **2012**, *67*, 93–104. [[CrossRef](#)]
44. Teluguntla, P.; Thenkabail, P.S.; Oliphant, A.; Xiong, J.; Gumma, M.K.; Congalton, R.G.; Yadav, K.; Huete, A. A 30-m landsat-derived cropland extent product of Australia and China using random forest machine learning algorithm on Google Earth Engine cloud computing platform. *ISPRS J. Photogramm. Remote Sens.* **2018**, *144*, 325–340. [[CrossRef](#)]
45. Pelletier, C.; Valero, S.; Inglada, J.; Champion, N.; Dedieu, G. Assessing the robustness of Random Forests to map land cover with high resolution satellite image time series over large areas. *Remote Sens. Environ.* **2016**, *187*, 156–168. [[CrossRef](#)]
46. Gong, P.; Wang, J.; Yu, L.; Zhao, Y.; Liang, L.; Niu, Z.; Huang, X.; Fu, H.; Liu, S. Finer resolution observation and monitoring of global land cover: First mapping results with Landsat TM and ETM+ data. *Int. J. Remote Sens.* **2013**, *34*, 2607–2654. [[CrossRef](#)]
47. Tong, X.; Brandt, M.; Hiernaux, P.; Herrmann, S.; Rasmussen, L.V.; Rasmussen, K.; Tian, F.; Tagesson, T.; Zhang, W.; Fensholt, R. The forgotten land use class: Mapping of fallow fields across the Sahel using Sentinel-2. *Remote Sens. Environ.* **2020**, *239*, 111598. [[CrossRef](#)]
48. Griffiths, P.; Nendel, C.; Hostert, P. Intra-annual reflectance composites from Sentinel-2 and Landsat for national-scale crop and land cover mapping. *Remote Sens. Environ.* **2019**, *220*, 135–151. [[CrossRef](#)]
49. Giri, C.; Pengra, B.; Long, J.; Loveland, T.R. Next generation of global land cover characterization, mapping, and monitoring. *Int. J. Appl. Earth Obs. Geoinf.* **2013**, *25*, 30–37. [[CrossRef](#)]
50. Verburg, P.H.; Neumann, K.; Nol, L. Challenges in using land use and land cover data for global change studies. *Glob. Chang. Biol.* **2011**, *17*, 974–989. [[CrossRef](#)]

Publisher’s Note: MDPI stays neutral with regard to jurisdictional claims in published maps and institutional affiliations.



© 2020 by the authors. Licensee MDPI, Basel, Switzerland. This article is an open access article distributed under the terms and conditions of the Creative Commons Attribution (CC BY) license (<http://creativecommons.org/licenses/by/4.0/>).